Petroleum Science 18 (2021) 1021–1032

Contents lists available at ScienceDirect

Petroleum Science

journal homepage: www.keaipublishing.com/en/journals/petroleum-science

Original Paper

Kinetics and fractionation of hydrogen isotopes during gas formation from representative functional groups

Shuang-Fang Lu [a], Guo-Qi Feng [a], Ming-Li Shao [b], Ji-Jun Li [a, *], Hai-Tao Xue [a], Min Wang [a], Fang-Wen Chen [a], Wen-Biao Li [a], Xiao-Ting Pang [a]

[a] Research Institute of Unconventional Oil & Gas and New Energy, China University of Petroleum, Qingdao, Shandong 266580, China
[b] Exploitation and Development Research Institude of Jilin Oilfield Company, CNPC, Songyuan, Jilin, 138000, China

ARTICLE INFO

Article history:
Received 9 April 2020
Accepted 17 December 2020
Available online 10 July 2021

Edited by Jie Hao

Keywords:
Gas-forming compounds
Pyrolysis
Hydrogen isotopes
Fractionation
Chemical kinetics

ABSTRACT

A gold tube simulation device was used to study the cleavage of representative compounds into gas. The goal of this study is to investigate hydrogen isotope composition change of gaseous hydrocarbons during maturity. Gas chromatography and isotopic analyses were conducted to determine how the yield of natural gas components and their hydrogen isotopic composition were related to experimental temperature and heating rate. A chemical kinetic model for the generation of each component of the natural gas and for the hydrogen isotopic fractionation was established and calibrated based on the results. Results indicate that the hydrogen isotopic fractionation during the evolution of various gas-forming organic materials can be satisfactorily described by chemical kinetic models. During regular methane generation, the reactions at low–activation–energy region had a greater contribution than the high–activation-energy region. While the reactions with high–activation-energy region had greater contribution of deuterium-rich methane. Compared with carbon isotope fractionation, this results in a greater hydrogen isotopic fractionation, which is more sensitive to changes in maturity. This study lays a foundation for further investigations of genesis and maturity of natural gas provided by hydrogen isotopic fractionation. It also provides fundamental knowledge for investigating the filling history of natural gas reservoir and for identifying.

1. Introduction

Natural gas is a mixture of hydrocarbons that contain fewer than five carbon atoms. It is unlike crude oil, which has complex compositions, rich in biomarkers (Peters et al., 2005) having abundant geochemical information. The relatively simple composition of natural gas makes it difficult to obtain generative information, such as the properties and thermal maturity of the gas, potential source rocks, migration pathways, mixed-source gas, and the accumulation history of gas reservoirs. The carbon and hydrogen isotopic compositions of natural gas components record information on the organic matter and source rocks, sedimentation environment, maturity, migration, mixing, aggregation, and dissociation history. The initial investigation and interpretation of this information was based on qualitative reasoning. For example, the bonds formed by light isotopes break preferentially, so light isotopes (e.g., ^{12}C versus ^{13}C) are concentrated in the gas products (Stahl 1974; Dai et al., 1989; Zhang, 1991; Carpentier et al., 1996; Xu et al., 2000; Cifuentes and Salata, 2001; Mazeas and Budzinski 2002; Métayer et al., 2014; Liu et al., 2018; Zhang et al., 2018). If the degree of enrichment in light isotopes (^{12}C, H) during this process can be calculated quantitatively, it can be used to more fully explore genesis and reservoir formation information. This has been demonstrated by quantitative simulations of the isotope fractionation for inorganic geochemical processes. Quantitative simulations of isotope fractionation in organic geochemistry also gradually demonstrate the research and application potential of this field (Berner et al., 1995; Rooney et al., 1995; Botz et al. 1996a, 1996b; Lorant et al. 1998, 2000; Cramer et al. 1998, 2001; Tang et al., 2000; Gaschnitz et al., 2001; Mazeas and Budzinski 2002; Shuai et al., 2003; Zou et al., 2003; Guan and Wu, 2003; Li et al., 2008; Xia and Tang 2012; Cai et al., 2013; Xia et al., 2014; Lu et al., 2015; Wang et al., 2015).

Currently, quantitative research on isotopic fractionation during hydrocarbon generation from organic matter is mainly focused on carbon isotopic fractionation processes (Rooney et al., 1995; Berner et al., 1995; Cramer et al., 1998; Lorant et al. 1998, 2000; Tang et al.,

* Corresponding author.
E-mail address: lijj@upc.edu.cn (J.-J. Li).

https://doi.org/10.1016/j.petsci.2020.09.001

2000; Gaschnitz et al., 2001). However, reports on the quantitative analyses of hydrogen isotopic fractionation are rare (Berner et al., 1995; Tang et al., 2005; Lu et al., 2011; He et al., 2019).

The lag in research on quantitative modeling of hydrogen isotopic fractionation may be due to limitations in available analytical techniques. The accuracy and reproducibility of early analyses of hydrogen isotopes were not high. In addition, there are more factors affecting the hydrogen isotopic compositions of organic matter. Possible exchange reactions between organic and inorganic hydrogen also make this research more complicated (Redding et al., 1980).

However, with improvements in analytical precision of hydrogen isotopes and the development of experimental methods, analytical techniques no longer restrict research in this field. The many factors affecting compositions of hydrogen isotopes also allow analysis of the effects of various factors based on hydrogen isotopic compositions. We must first quantitatively identify the degree of influence that the various factors have on the hydrogen isotopic composition. A study of the chemical kinetics of hydrogen isotopic fractionation during the formation of gas from organic matter meets this quantitative requirement well.

The relative mass differences between the two stable isotopes of hydrogen (H, 99.985%; ^{2}H, 0.015%) is the largest of all the elements, thus hydrogen has the most variable stable isotope ratio range (Wang 1996). For example, hydrogen isotopic compositions of methane in China range from −83‰ to −312‰ (Dai et al., 1993). Globally reported δ^2H values are between −16‰ and −470‰ (Wang et al., 2004). This unique characteristic makes the composition of hydrogen isotopes a sensitive geochemical indicator that can provide geological information.

Many previous studies concluded (Tang et al., 2000) that due to the heterogeneity of the structure of organic matter, complex changes are usually observed during isotopic fractionation. Generally, the heterogeneity of isotope distributions in organic matter is mainly affected by ring structures, aromatic ring structures, and heteroatoms (O, N and S). For example, the groups linked to heteroatoms tend to be enriched with heavy (carbon) isotopes. Therefore, in this study, the major gas-forming functional groups of organic matter were represented by chain hydrocarbons, naphthenes, aromatic hydrocarbons, or compounds containing heteroatoms to avoid the influence of isotope distribution heterogeneities in organic matter on the quantitative modeling of isotopic fractionation. Since there are many compounds in each category, the gas-forming selected compounds were chosen so that they have similar numbers of carbon atoms, and so that the cyclic naphthenes and aromatic hydrocarbons do not contain side chains, which allows better comparisons. According to this principle, octadecane, octadecanoic acid, and octadecylamine with 18 carbon atoms each were selected to represent the chain hydrocarbons, oxygen-containing compounds, and nitrogen-containing compounds, respectively. In addition, 9-phenylhydrazine with 20 carbon atoms was selected to represent the aromatic compounds; decahydronaphthalene was selected to represent the naphthenes because appropriate chemically pure cyclic compounds with 18 carbon atoms are not easily obtained. Simulation experiments on gas formation from pyrolysis were then conducted to determine how the production yield of natural gas components and their hydrogen isotopic composition were related to the experimental temperature and heating rates. The characteristics of the different gas-forming functional groups were compared. Kinetic models for gas formation and the chemical kinetic models for isotopic fractionation were also established and calibrated. This study provides new technical methods and insights into the study of the different genetic types of natural gas, sources of precursors, determination of maturity, and the history of reservoir formation. The results of hydrogen isotopic fractionation and its chemical kinetics during gas formation are reported in this study.

2. Materials and methods

2.1. Materials

The molecular formulas and initial hydrogen isotope for the five selected representative gas-forming functional groups are listed in Table 1.

2.2. Methods

Gold tube thermal simulation experiments have gained popularity in recent years (Sajgó et al., 1986; Landais et al., 1994; Schenk et al., 1997; Liu and Tang 1998, 2000; Tang et al. 2000, 2005; Xiong et al., 2001; Guo et al., 2009; Jin et al., 2010). The advantage of gold tube experiments is that the pressure can be set and regulated and is very flexible because of the plasticity of the gold tube. In addition, the applied pressure is exactly the reaction pressure in the pores required for this study.

The thickness of the gold tubes used in the experiments was 0.2 mm, the outer diameter was 4 mm, and the maximum volume was 1 cm^3. The amount of sample ranged from 5 to 100 mg. Once it was filled with sample, the gold tube was placed in an argon box to remove air in the tube, and then the tube was sealed using a high-frequency welder (Lu et al., 2011). The sealed gold tube was transferred into an autoclave with water as the pressure medium. Multiple autoclaves could be used simultaneously in this experiment. Each autoclave was connected to a shut-off valve and was then connected to the same pressure system. The system pressure could be set to certain values using a pressure control system, and the accuracy of the pressure gauge was ±0.5 MPa. The autoclaves were placed in a water tank which can maintain the set temperature, and the water tank could be heated at a constant heating rate. The accuracy of the temperature controller was ±0.1 °C. Therefore, all of the gold tubes were subjected to the same pressure and temperature. The pressure and temperature systems were controlled by a central control computer (Lu et al., 2011).

The samples were heated at 50 MPa from 200 °C to 600 °C at a heating rate of either 20 °C/h or 2 °C/h. Each shut-off valve connected to the autoclave was closed at a certain target temperature, after which the autoclave was taken out of the incubator, and the gold tube was taken out of the autoclave after it cooled. The gold tube was then placed in a special gas collection system for accurate measuring. After it was opened in vacuum, the gases (including hydrocarbon gases $C_{1\text{-}5}$ and non hydrocarbon gases such as CO_2, H_2 and H_2S) in gold tube was quantitatively analyzed using an HP 6890 gas chromatograph (GC) as described by Lu et al. (2019).

The remaining gas was sampled using a gas-tight syringe for hydrogen isotope analysis using a Finnigan DELTA Plus XL from Finnigan Co. The GC used was an Agilent 6898. A ParaPlot Q, 25 m × 0.32 mm × 0.25 μm column was used. The initial temperature was 50 °C for 10 min, and then, the column was heated at

Table 1
Molecular formulas and initial hydrogen isotopic compositions of representative gas-forming compounds.

Gas-forming compounds	Molecular formula	Initial δ^2H, ‰
Octadecane	$C_{18}H_{38}$	−114.480
Octadecanoic acid	$C_{18}H_{36}O_2$	−131.110
Decahydronaphthalene	$C_{18}H_{39}N$	−143.100
Octadecylamine	$C_{10}H_{18}$	−243.315
9-Phenylhydrazone	$C_{20}H_{14}$	39.400

10 °C/min to 180 °C, which was maintained for 15 min. The column flow rate was 1 ml/min. Hydrogen isotope values is referenced to the SMOW (standard mean ocean water) standard, which is defined as $\delta^2H = 0‰$, and its absolute hydrogen isotope ratio $^2H/H=(155.76 \pm 0.10) \times 10^{-6}$. The hydrogen isotope value of each sample was measured two times or more and the measurement precision is within ±3.0‰.

3. Results and discussion

3.1. Characteristics of gaseous compounds formed by representative compounds

The relationship between the yield of the main products (methane, heavy hydrocarbon gas, hydrogen, and CO_2) formed during pyrolysis of the five representative gas-forming compounds (octadecane, octadecylamine, octadecanoic acid, decahydronaphthalene, and 9-phenylanthracene) and the temperature/heating rate was reported separately (Lu et al., 2019) and will not be discussed in this study. The characteristics were similar to those of most gas-formation simulation experiments. The methane yield increased gradually, and the heavy hydrocarbon gas (C_{2-5}) yield initially increased and then decreased with increasing degree of evolution. Generally, the final gas yield was determined by the effective hydrogen atom content in the functional groups. The time and difficulty of gas formation was determined by the structure of the reactants. The chain-structured compounds (octadecane, octadecylamine, and octadecanoic acid) started to form gas earlier, while the cyclic compounds (decalin and 9-phenylanthracene) started to produce gas relatively late. This is partially due to high thermal stability of the cyclic compounds because rings have to be opened before gas formation can occur.

3.2. Hydrogen isotopic fractionation during formation of gas from representative compounds

Fig. 1 shows the relationship between the hydrogen isotopic composition (δ^2H) and the pyrolysis temperature/heating rate during pyrolysis of the five main gas-forming functional groups (octadecane, octadecylamine, octadecanoic acid, decalin and 9-phenylanthracene) to form methane. Fig. 1 shows that the δ^2H values of each component generally increase with increasing temperature which is consistent with previous research resluts from thermal simulation experiments and natural gas (Ni et al. 2011, 2013; He et al. 2018, 2019). However, the δ^2H of methane from the pyrolysis of compounds with heteroatoms or ring structures (octadecylamine, octadecanoic acid, and decahydronaphthalene) exhibit a downward trend during the early stage of evolution. No δ^2H value was obtained for 9-phenylanthracene because there was low gas yield during the early stage of evolution. It is therefore unclear whether the δ^2H value of the methane produced decreases during the early stage of evolution. The above result is consistent with the decrease in $\delta^{13}C_1$ frequently observed in gas formation experiments. The decrease in the δ^2H value can be explained by the heterogeneity of the hydrogen isotopic composition of the sample, which is similar to the change in $\delta^{13}C_1$ observed during thermal evolution (Rooney et al., 1995; Lorant et al., 1998; Tang et al., 2000; Cramer et al., 2001; Lu et al., 2011). The heterogeneity of the hydrogen isotope distribution is caused by the presence of heteroatoms or cyclic structures in the compounds. Deuterium (^2H) may be relatively concentrated on carbon atoms adjacent to or close to the heteroatoms. The δ^2H of methane initially generated was high because the heteroatom-related groups were easy to break. With increasing temperature, the influence of the heteroatoms gradually weakened and disappeared. Therefore, the methane formed later contained less ^2H than methane formed earlier, and the δ^2H values exhibited a downward trend. As temperature increases, ^2H gradually becomes enriched during subsequent methane production. Because the binding force of the C—C bond in the organic precursors, which are composed of ^2H-containing groups ($-CH_2^2H$) is stronger than that of $-CH_3$ groups. As a result, ^2H in the residual precursor is gradually enriched due to the release of ^2H-depleted products previously, and the generated methane in later stage is more enriched with ^2H. Unlike the apparent initial decrease in $\delta^{13}C$ during the formation of methane from octadecane (Lu et al., 2011), there was no initial decrease in δ^2H during methane formation. In the carbon isotope fractionation process, the bond dissociation energy ($\Delta\Delta H$) and the isotope fractionation factor show a weak negative correlation, which indicates that the cleavage of methyl group from NSO precursors has weaker carbon isotopic fractionation effect than that from C—C cracking at higher maturity. This is the main reason for the rollover of $\delta^{13}C_1$ at early maturation stages. On the contrary, there is a positive correlation between $\Delta\Delta H$ with the isotope fractionation factor during hydrogen isotope fractionation process. This result will lead to the gradually enrichment of ^2H in methane and no initial decrease of δ^2H_1 during maturation (Tang et al., 2000; He et al., 2018).

Table 2 summarizes the distribution and fractionation range of δ^2H in the gaseous products generated by the gas-forming compounds. As shown in Fig. 1 and Table 2, the observed fractionation range of δ^2H for methane in the experiment was 129 ‰–255‰, which was much higher than that of the $\delta^{13}C$ for methane, which does not generally exceed 30‰ during the evolution process (Lorant et al. 1998, 2000; Cramer et al. 1998, 2001). The fractionation ranges of the ethane and propane were 159 ‰–267‰ and 138 ‰–245‰, respectively, which are also far higher than those for the $\delta^{13}C$ values (approximately 40‰). Therefore, the sensitivity of δ^2H values to isotopic fractionation makes δ^2H a potential indicator of maturity.

It can also be seen from Tables 1 and 2 that the δ^2H_1 values of

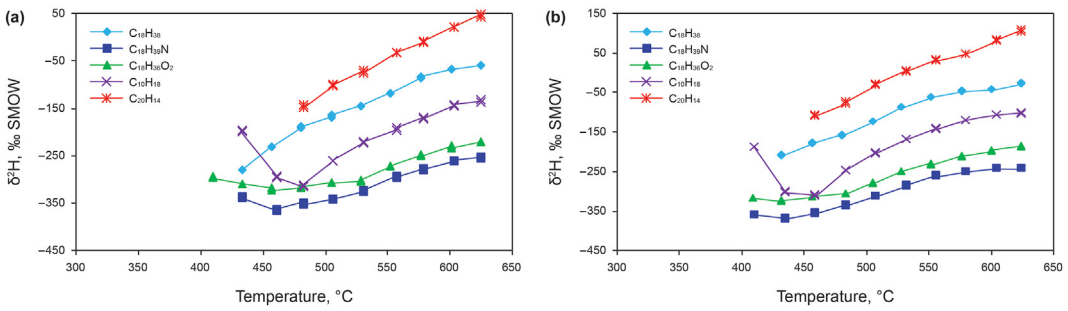

Fig. 1. δ^2H values of compounds from the various representative methane-forming functional groups as a function of temperature at heating rates of (a) 20 °C/h and (b) 2 °C/h.

Table 2
Fractionation range of δ^2H in products of representative gas-forming functional groups.

Gas-forming functional groups	Experimentally observed fractionation range of δ^2H of methane, ‰	Experimentally observed fractionation range of δ^2H of ethane, ‰	Experimentally observed fractionation range of δ^2H of propane, ‰
Octadecane	253	267	245
Octadecanoic acid	137	198	199
Decahydronaphthalene	212	220	189
Octadecylamine	129	204	138
9-Phenylhydrazone	255	159	n.d.

n.d. – not detected.

methane, the final hydrocarbon product, are much higher than the original δ^2H_1 values. This differs from the $\delta^{13}C_1$ values of the final hydrocarbon product, methane, which are generally not higher than the original values (Lorant et al. 1998, 2000; Cramer et al. 1998, 2001). This means that the residual samples, the heavy hydrocarbon intermediates, or the hydrogen products may be relatively enriched with the light hydrogen isotope, protium, which is consistent with the principle of isotopic mass balance. Simple calculations based on the principle of material balance indicate that the hydrogen was transferred to the pyrolysis product at temperatures above 500 °C, and the residual organic matter was usually free of hydrogen. Taking octadecane as an example, the hydrogen content per gram of octadecane is 150 mg based on elemental compositions. The total mass of hydrogen in the gases (hydrocarbon gas + hydrogen gas) generated during the pyrolysis of octadecane was approximately 150 mg after the experimental temperature reached 500 °C as shown in Fig. 2, which is consistent with the calculated result. There was more deuterium in the heavy hydrocarbon gas than in the methane gas as shown in Table 2, Fig. 3, and Fig. 4 (The detailed isotopic data have been reported in Appendix Table 1). Therefore, only the hydrogen gas could become enriched in the lighter hydrogen isotope (H). Unfortunately, no δ^2H values were obtained for hydrogen due to analytical constraints. This is also consistent with the principle of isotopic fractionation because methane is not the final product of the hydrogen's evolution, while hydrogen is the most stable form. Therefore, as predicted by the principle of isotopic fractionation (light isotopes are preferentially enriched in the volatile products), most of the H is transferred to the hydrogen gas, resulting in the δ^2H values of the methane being higher than the original δ^2H values. However, in the case of carbon isotopes, methane is the final form of stable hydrocarbon gas, so the $\delta^{13}C$ of the methane cannot be higher than the original $\delta^{13}C$.

Table 1 and Fig. 1 also show that the order of the δ^2H values of the original gas-forming functional groups (from light to heavy: octadecylamine, decalin, octadecanoic acid, octadecane, and 9-phenylanthracene) is different from the order of the upper limit of the δ^2H values of the final hydrocarbon product, methane (from light to heavy: octadecylamine, octadecanoic acid, decalin, octadecane, and 9-phenylanthracene). A similar inconsistency was observed for the carbon isotopic compositions of the methane generated from the five functional groups. However, the δ^2H values of the methane gas produced from the different gas-forming functional groups with chain structures showed an inheritance effect. The order of the δ^2H values of the methane produced from light to heavy is consistent with that of the δ^2H values for the original compounds (from light to heavy: octadecylamine, octadecanoic acid, and octadecane). The decahydronaphthalene and 9-phenylanthraquinone have ring structures and aromatic ring structures, respectively. The order of the δ^2H values of their products is consistent with the order of their original δ^2H values, but they exhibit a different inheritance effect with the chain hydrocarbons. This is also consistent with the $\delta^{13}C_1$ results obtained during evolution. In general, octadecylamine and octadecanoic acid have a smaller fractionation range (<140‰), while the other three natural gas-forming functional groups have a larger fractionation range (>210‰). However, the range of hydrogen isotopic fractionation during gas formation from the heteroatom-containing groups needs to be validated with more evidence and data from further experiments.

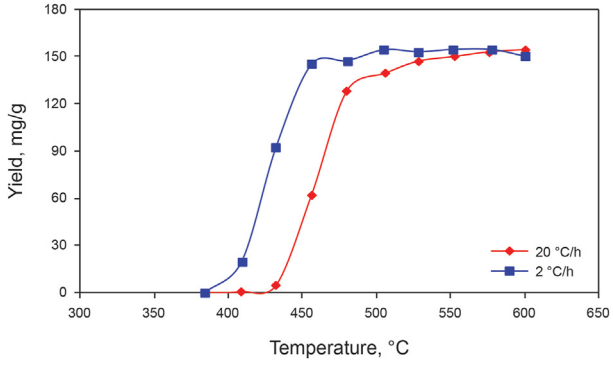

Fig. 2. Total mass of hydrogen atom in hydrocarbon gas + H_2 gas generated by pyrolysis of octadecane.

Figs. 3 and 4 show the hydrogen isotopic compositions (δ^2H) of ethane and propane, respectively, from pyrolysis of the five gas-forming compounds. The δ^2H_2 and δ^2H_3 of all of the products were generally lower to higher for octadecylamine, octadecanoic acid, decahydronaphthalene, octadecane, and 9-phenylanthraquinone, which is consistent with the order of the δ^2H_1 value of methane. δ^2H_2 of the ethane during the pyrolysis of octadecylamine, octadecanoic acid, decahydronaphthalene, and octadecane gradually decreased during the late stage of evolution, which is not consistent with the evolution trend of δ^2H_1 (because of the further cracking that occurs at higher temperatures, the δ^2H_3 values obtained for propane were not enough to establish an evolutionary trend). This decrease is consistent with the obvious decrease observed in the carbon isotope values of ethane at high temperatures. Therefore, the mechanism used to explain the change in $\delta^{13}C_2$ can also possibly be applied to the change in δ^2H. The cleavage of alkylaromatics could be one of the main sources of gaseous hydrocarbons during the later stages of evolution, and the dealkylation and ring-opening reactions that occur at this time could lead to a lower isotopic composition of the gaseous hydrocarbons (Lorant et al. 1998, 2000). Unlike methane in closed systems, where the decrease of δ^2H is absent due to cumulative effects, the carbon isotopes of the small amount of generated ethane became lighter, and this is reflected by the δ^2H_2 values because ethane generated in the early stages was mostly cracked by this time.

The hydrogen isotopic compositions of the methane, ethane, and propane generated from each gas-forming functional group are plotted in Figs. 5–9. In general, the hydrogen isotopic compositions of the hydrocarbon gases produced from the precursors of the chain structure conformed to the regular isotopic sequence of

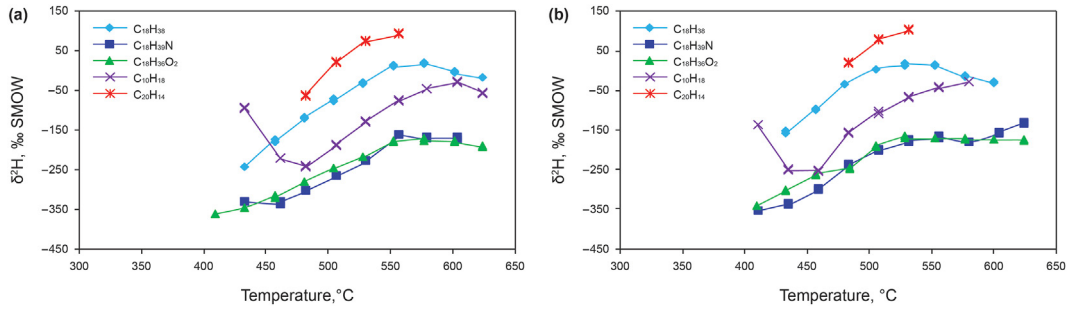

Fig. 3. δ^2H values of ethane generated from pyrolysis of compounds with different functional groups at heating rates of (a) 20 °C/h and (b) 2 °C/h.

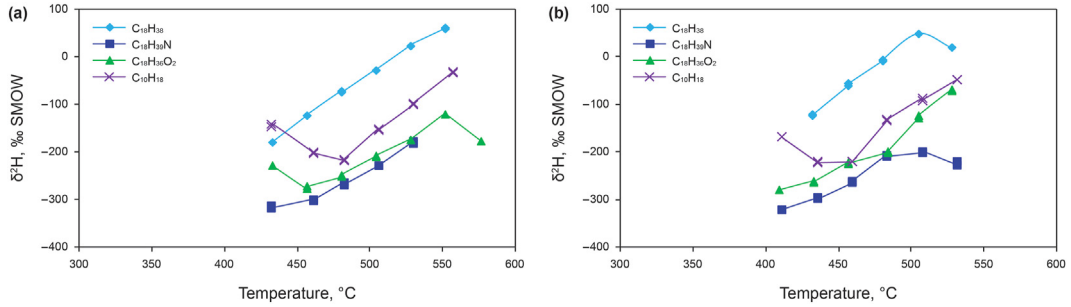

Fig. 4. δ^2H values of propane generated from pyrolysis of compounds with different functional groups at heating rates of (a) 20 °C/h and (b) 2 °C/h.

$\delta^2H_1<\delta^2H_2<\delta^2H_3$, which is consistent with the characteristics of hydrogen isotope distribution of natural gases under geological conditions. A few of the experimental data points exhibit some inversion of the sequence because of the decrease in δ^2H in the early and late stages. However, the inversion of δ^2H_2 and δ^2H_3 for decahydronaphthalene, which has a ring structure, is a relatively common phenomenon. It is difficult to present a persuasive explanation for this phenomenon because the relative probability distributions of ^2H and H in the ring structure cannot be obtained. However, it can be stated that the inversion of the carbon isotopes does not necessarily indicate the formation of inorganic gases, not does the inversion of hydrogen isotopes. 9-Phenylanthraquinone, which has an aromatic structure, produced less propane. The corresponding δ^2H_3 value was not obtained, and thus it is unknown whether the δ^2H_2 and δ^2H_3 values were inverted.

The compositions and fractionation of hydrogen isotopes exhibit characteristics like those of the carbon isotopes during gas formation from the representative gas-forming compounds. This may indicate that the mechanisms for hydrogen and carbon isotopic fractionation during the evolution of organic matter into gas are similar, which could provide some guidance for the quantitative analysis of hydrogen isotopic fractionation.

3.3. Chemical kinetic model and its calibration for hydrogen isotopic fractionation

3.3.1. Models

Although kinetic models for carbon isotopic fractionation have been widely discussed and successfully applied (Rooney et al., 1995; Berner et al., 1995; Cramer et al., 1998; Lorant et al. 1998, 2000; Tang et al., 2000; Gaschnitz et al., 2001), there are few reports on the quantitative characterizations of hydrogen isotopic fractionation (Berner et al., 1995; Lu et al., 2011). Our group has used the same model for carbon isotopic fractionation to quantitatively describe hydrogen isotopic fractionation based on similarities in characteristics and mechanisms for fractionation of carbon isotopes and hydrogen isotopes.

The carbon isotopic fractionation models reported in various studies are different, but can be divided into two broad categories based on their basic principles: fractionation models based on the Rayleigh equation and chemical kinetic models based on the kinetics of formation of light and heavy carbon isotopes.

As has been verified by our group (Lu et al., 2006), the latter model, in particular the Cramer model III in which the ^{12}C and ^{13}C generation are considered as two parallel and related processes, has more extensive applicability compared to the other carbon isotopic

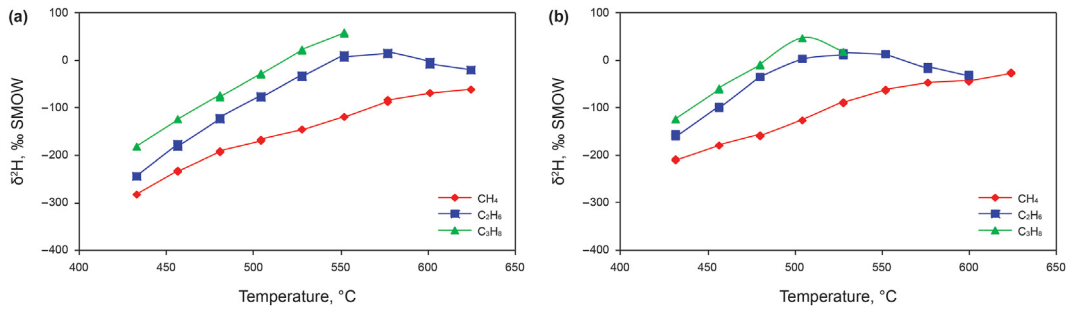

Fig. 5. The relationship of δ^2H values among gaseous hydrocarbons in the pyrolysis of octadecane at heating rate of (a) 20 °C/h and (b) 2 °C/h.

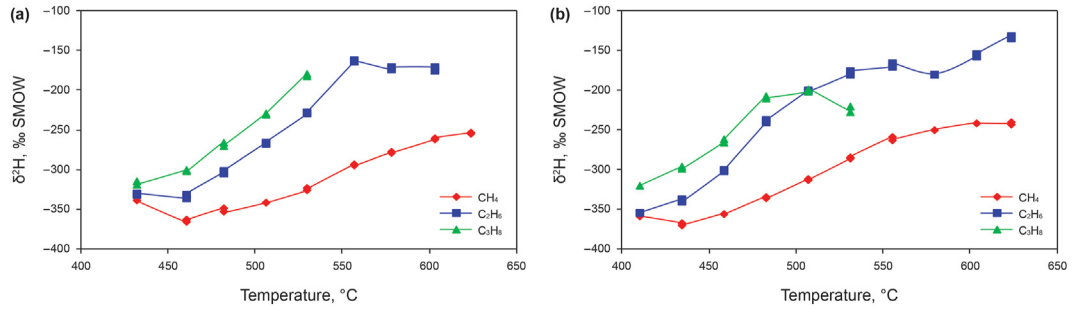

Fig. 6. The relationship of δ^2H values among gaseous hydrocarbons in the pyrolysis of octadecylamine at heating rate of (a) 20 °C/h and (b) 2 °C/h.

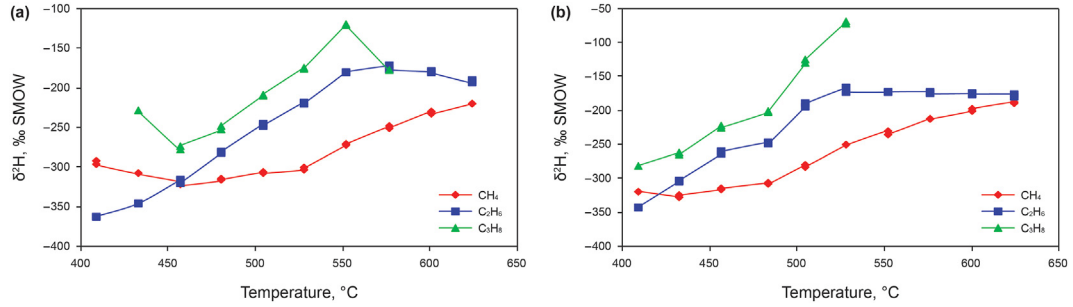

Fig. 7. The relationship of δ^2H values among gaseous hydrocarbons in the pyrolysis of octadecanoic acid at heating rate of (a) 20 °C/h and (b) 2 °C/h.

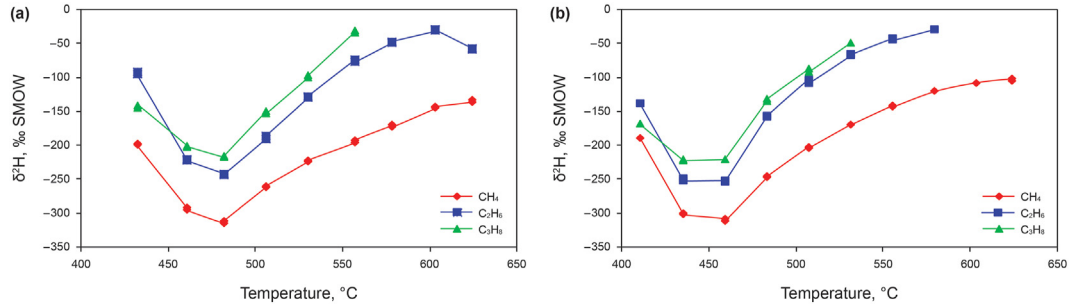

Fig. 8. The relationship of δ^2H values among gaseous hydrocarbons in the pyrolysis of decahydronaphthalene at heating rate of (a) 20 °C/h and (b) 2 °C/h.

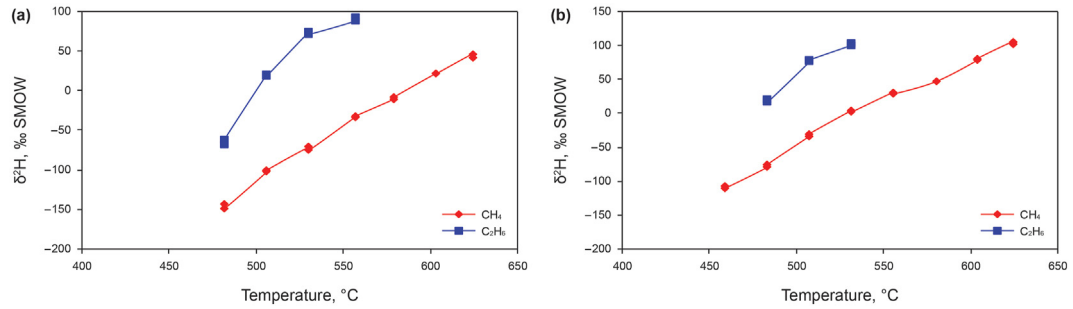

Fig. 9. The relationship of δ^2H values among gaseous hydrocarbons in the pyrolysis of 9-phenylhydrazine at heating rate of (a) 20 °C/h and (b) 2 °C/h.

fractionation models. Cramer model regards methane generation as the result of n parallel first-order reactions. For each reaction, the generation rate coefficients of heavy isotope component (such as CH_3^2H) and normal isotope component (such as CH_4) are different. Firstly, the conversion curve of gas generation is fitted to optimize the kinetic parameters, which are used as those of predominant normal isotope component. After that, for Cramer I and Cramer II models, the activation energy difference (ΔEa) between heavy and normal isotope components is optimized to fit gas isotope value. The difference is that ΔEa for each parallel reaction is a fixed value in Cramer I model, but the value is variable in Cramer II model. For Cramer III model, the independent kinetic parameters of CH_3^2H were optimized to fit isotope values of methane (Cramer et al. 1998, 2001; Shuai et al., 2003).

3.3.2. Model calibration

The gas-forming conversion rate at each point can be obtained from the ratio of the gas yield of each experimental point to the maximum gas yield (calculated from the elemental composition of nC_{18} and the elemental composition of the methane product based on the principle of material balance). The resulting curves show the relationship between the gas-forming conversion rate and temperature. Since H_1 accounts for most hydrogen gas, the curve of H_1 can be regarded as the generation curve for CH_4. The generation curve for CH_3^2H can be obtained by calculating the amount of CH_3^2H generated at each experimental point based on the δ^2H value. On this basis, the kinetic parameters for the generated CH_4 and CH_3^2H can be calibrated separately. The generation curve and kinetic parameters together comprise the chemical kinetic model for hydrogen isotopic fractionation during the formation of gas from organic matter. Hence, the amount of CH_4 and CH_3^2H produced and the corresponding hydrogen isotopic composition under any conditions can be calculated.

According to this principle, hydrogen isotopic fractionation during the formation of gas from organic matter can be calculated by separately calibrating the kinetic models for the generation of CH_4 and CH_3^2H. However, the obtained model fits both the isotopic fractionation curve and the gas-generation curve (Fig. 1). The basic principles and methods of model calibration have been reported in previous studies and are not discussed here (Lu et al., 2011).

3.3.3. Model-calibration results

Based on our trial calculations and our accumulated experience in the calibration of kinetic models for the generation of hydrocarbons, pre-exponential factors for the pyrolysis of all samples into H-methane were set at 6×10^{14}/min in order to compare the calibration results. However, since the relative mass difference between H and ^2H is the largest among all isotopes, they have the largest relative activation-energy difference, and, correspondingly, they should also have a large difference in their pre-exponential factors. For the frequency factor ratio of carbon isotopic fractionation, potential energy difference between the transition state and the final product is small. Therefore, exact location of the transition state is not required, and the frequency factor ratio can be determined to be 1.02 (Tang et al. 2000, 2005). But for hydrogen isotope fractionation, the potential energy difference is significant and that the approach of using two radical energies for approximating the transition barrier is not valid. In order to obtain correct frequency factor ratio for hydrogen isotope fractionation, the transition state must be located to obtain an accurate transition barrier energy. Using a transition state calculation, the hydrogen isotope effect on the frequency factor ratio for homolytic bond rupture is 1.07 (Ni et al., 2011). According to the above-described principle, the resulting calibrated activation energy distributions of each representative compound for the generation of H-methane and ^2H-methane are plotted in Fig. 10 (The detailed activation energy distributions have been reported in Appendix Table 2).

Table 3 summarizes the average-activation energy and activation energy difference between the generation of H-methane and ^2H-methane for each representative functional group. As shown in Fig. 10 and Table 3, the average activation energy of the reaction producing ^2H-methane is generally higher than that producing H-methane, which indicates that it is more difficult to break the C–C bond in ^2H–C–C–H than the C–C bond in H–C–C–H. Overall, the gas-formation potential (reaction fraction) of H-methane in the low-activation-energy region is higher than that of ^2H-methane, while in the high-activation-energy region the reaction fraction of ^2H-methane is higher. It is the above differences in the average activation energies and their distribution that result in the difference in the rate of formation of H-methane and ^2H-methane, which results in hydrogen isotopic fractionation during methane formation. Additionally, the calibrated results reveal that difference in the pre-exponential factors and activation energy distributions of the formation of ^{12}C and ^{13}C-containing methane in the carbon isotopic fractionation model is small (usually $E^{13}C_1 - E^{12}C_1 < 1$ kJ/mol), which has been reported by our group and other researchers (Cramer et al., 2001; Li et al., 2008). In contrast, the difference between H-methane and ^2H-methane is relatively large ($E^2H_1 - EH_1 > 2$ kJ/mol; Table 3). This leads to greater hydrogen isotopic fractionation, which is the reason the hydrogen isotopic composition is very sensitive to changes in temperature (maturity).

Based on previous results for the pyrolysis of organic matter from source-rocks pyrolysis of oil into gas, the gas-forming compounds with relatively simple compositions have a narrow distribution of activation energies (Lu et al., 2011). However, the average activation energy is relatively high. This is mainly related to the fact that there are only a few heteroatoms, but there are many C–C structures within the gas-forming compounds in this study, thus making them difficult to crack gas. This is also consistent with previous reported results (Ungerer 1990; Burnham et al., 1995; Schenk and Dieckmann 2004).

The yield curves for H-methane and ^2H-methane for the same experimental heating rate and heating temperatures were easy to calculate based on their chemical kinetic parameters (activation energy, pre-exponential factor, and reaction fraction of each reaction). By combining the yield curves with the ratio of the gas-formation potentials of H-methane and ^2H-methane (Table 3), the evolution curve of hydrogen isotopes can be calculated (Fig. 11). It can be seen that the calculated values from the model are in good agreement with the experimental values. This provides the basis and prerequisite for the application of the kinetic model of hydrogen isotopic fractionation under geological conditions, and it also lays the foundation for geological applications. Based on geological conditions (e.g., history of sedimentation and burial and thermal history) of a specific area, the hydrogen isotopic composition and evolution during natural gas formation can be calculated, which provides information necessary for investigation of the genesis and accumulation information of natural gas. This study also lays the foundation for exploratory applications on the history of gas reservoir formation and gas and source rock correlation.

4. Conclusions

(1) This study indicates that the hydrogen isotopic composition of natural gas is closely related to the following factors:

i) The degree of thermal evolution of organic matter. δ^2H of methane during the main gas-formation stage gradually increases with increasing experimental temperature. The fractionation range of δ^2H for methane is 129 ‰–255‰. This is much higher than range for the $\delta^{13}C$ of methane, which generally does not exceed 30‰. The δ^2H fractionation ranges of ethane and propane are 159 ‰–267‰ and 138 ‰–245‰, respectively, which are also far higher than that of $\delta^{13}C$ (about 40‰). This demonstrates the sensitivity of hydrogen isotopic composition as an indicator of maturity. However, δ^2H is likely to be lower in the early or late stages of evolution for compounds containing heteroatoms or ring structures which may be due to the heterogeneity of the hydrogen isotopic composition. Nevertheless, due to the relatively small amount of gas formed in the early and late stages, this has little effect on the overall isotopic composition of natural gas under geological conditions.

ii) The initial hydrogen isotopic composition of the reactants. In general, the hydrogen isotopic composition of

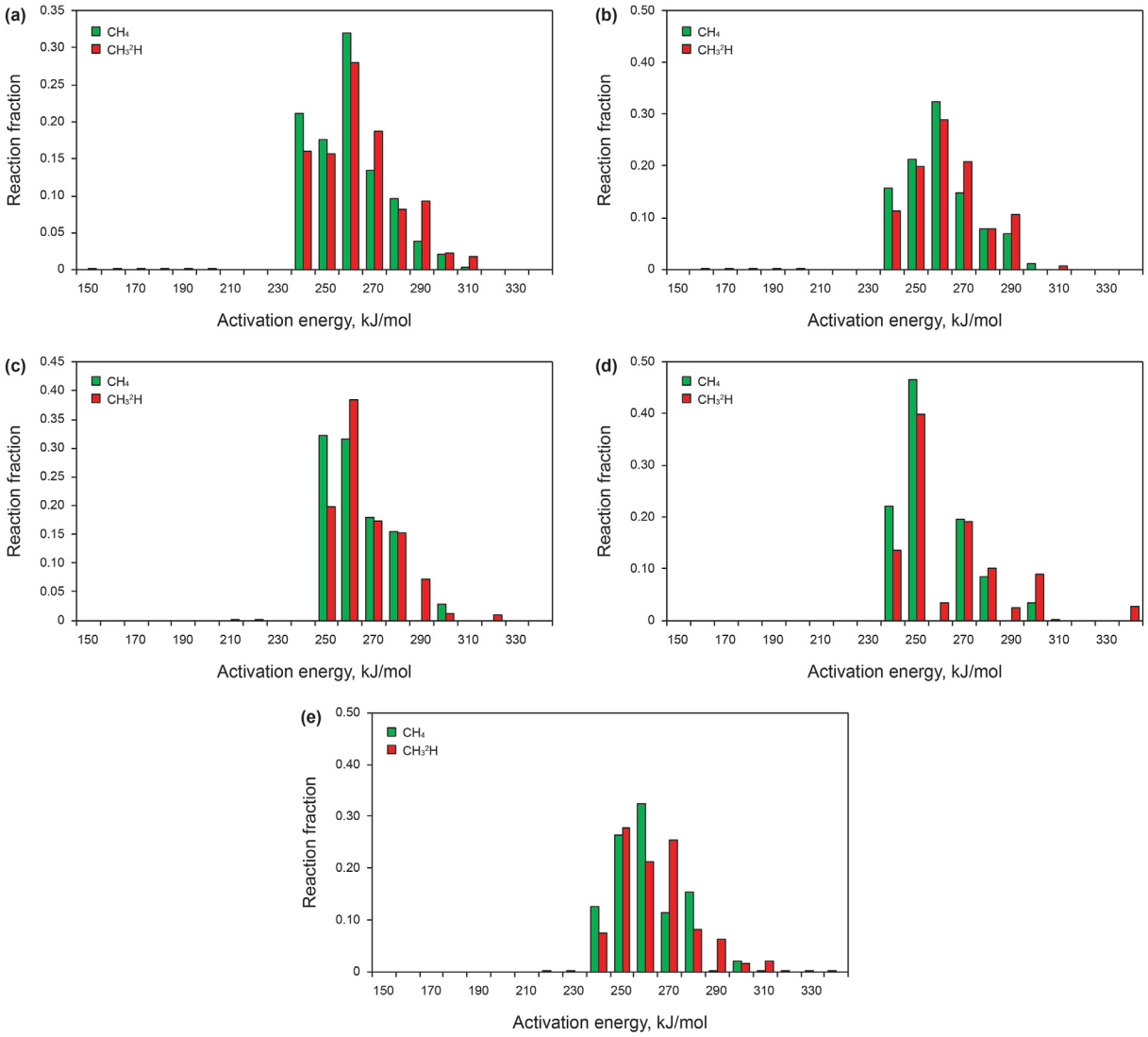

Fig. 10. Distribution of activation energies of pyrolysis of representative functional groups forming H- and ^{2}H-methane. (a) Octadecanoic acid, (b) octadecylamine, (c) decahydronaphthalene, (d) 9-phenylhydrazone, and (e) octadecan.

Table 3
Ratio of gas-formation potential and kinetic parameters of representative gas-forming compounds for the formation of H-methane (CH_4) and ^{2}H-methane (CH_3^2H).

Experiments	Ratio of gas-formation potential	$\overline{E_H}$, kJ/mol	$\overline{E_{^2H}}$, kJ/mol	$A_{^2H}/A_H$	$\overline{E_{^2H}} - \overline{E_H}$, kJ/mol
Octadecane	153.42×10^{-6}	259.87	263.48	1.07	3.62
Octadecanoic acid	127.72×10^{-6}	259.39	263.32	1.07	3.93
Octadecylamine	140.18×10^{-6}	260.35	262.92	1.07	2.57
Decahydronaphthalene	118.38×10^{-6}	262.74	265.99	1.07	3.24
9-Phenylhydrazone	179.12×10^{-6}	256.04	263.66	1.07	7.62

$\overline{E_H}$ is the average active energy of the generation of H-methane (CH_4).
$\overline{E_{^2H}}$ is the average active energy of the generation of ^{2}H-methane (CH_3^2H).

gaseous hydrocarbons is inherited from the precursors. This phenomenon is similar to that occurring in carbon isotopes. However, like the inheritance effect of carbon isotopes, this is mainly reflected in compounds with similar structures and, thus, similar gas-generation mechanisms. For example, octadecane, octadecanoic acid, and octadecylamine have the same number of carbon atoms and similar chain structures, and the mechanisms of the gas formation reactions are similar, so the inheritance effect of hydrogen isotopic composition was observed. However, the carbon isotopic composition of the hydrocarbon gas generated by gas-forming compounds with different structures does not necessarily have a comparable inheritance effect. This provides a reference for understanding the complexity of hydrogen isotopic fractionation during the formation of gas from oil and organic matter in source rocks.

iii) The structure of gas-formation precursors and the mechanism of the gas-formation reaction. Differences in the inheritance effects and fractionation trends between

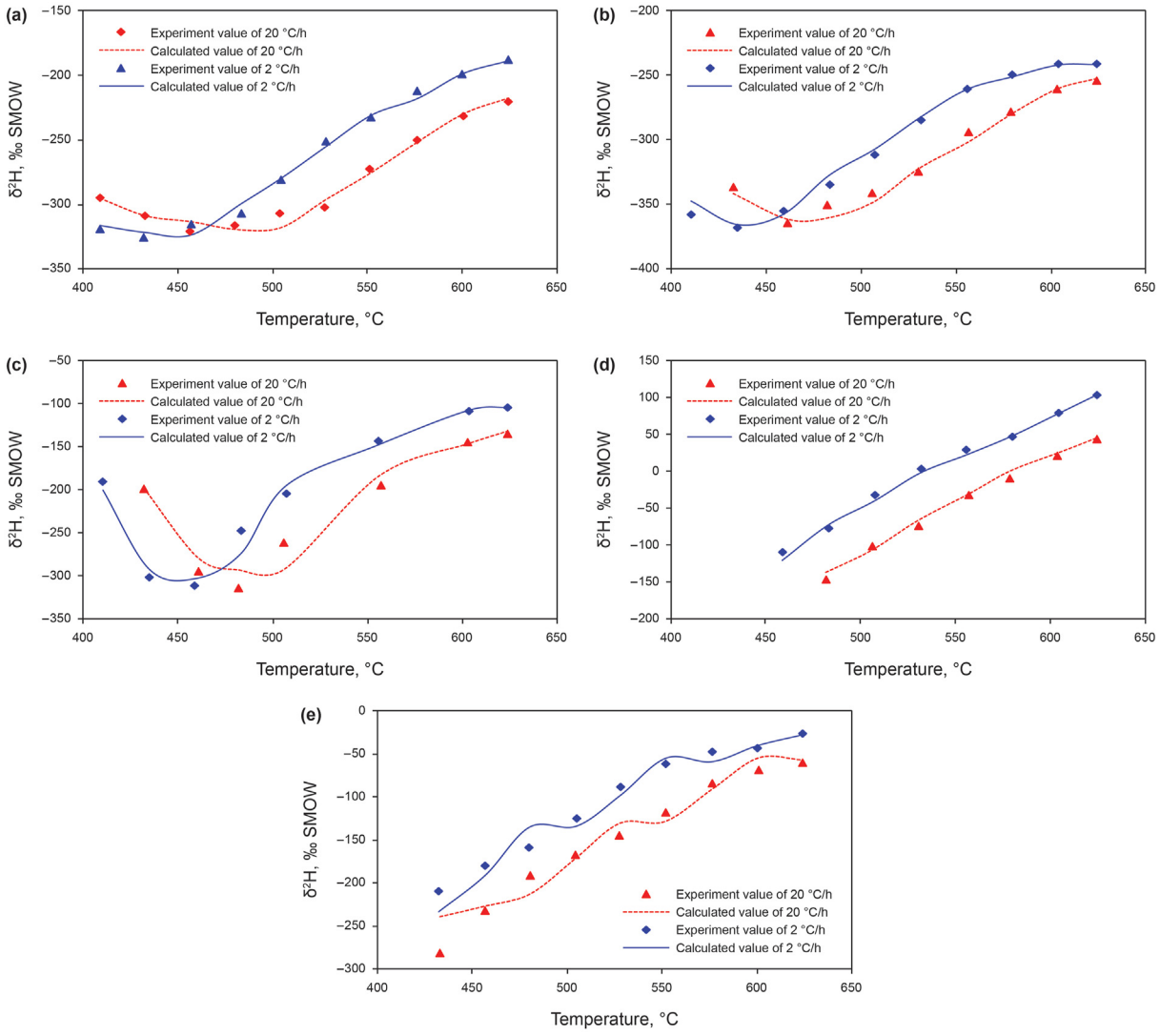

Fig. 11. Evolution curves of hydrogen isotopes during pyrolysis of representative gas-forming compounds to form methane. (a) Octadecanoic acid, (b) octadecylamine, (c) decahydronaphthalene, (d) 9-phenylhydrazone, and (e) octadecan.

compounds with chain structures and those with cyclic structures were observed in this study, which indicates that the structure of the gas-forming precursor has a significant effect on the degree of hydrogen isotopic fractionation. Different structures may yield different gas-forming reaction mechanisms. For example, when 9-phenylhydrazine (with aromatic structure) is heated, methane forms by the typical polycondensation reaction mechanism of aromatics. However, during the moderate-low-temperature stage of pyrolysis of octadecane, a chain structure compound, a simple C–C bond cleavage process occurs. During high temperature pyrolysis, octadecane will also produce (alkyl) aromatics as the result of disproportionation reactions, so there will also be an aromatics polycondensation reaction mechanism. With increasing pyrolysis evolution (temperature), the proportion of polycondensation reactions in octadecane continues to increase, and the polycondensation reactions dominate at high temperatures.

(2) The δ^2H_1 value for methane, the final hydrocarbon gas product, can be much higher than the original value, which contradicts the results for $\delta^{13}C_1$. This is because methane is not the final product in the evolution of hydrogen. Hydrogen gas is its most stable form. Therefore, based on the principle of isotopic fractionation, the light isotopes are preferentially enriched in the final product, so more H is transferred to the hydrogen gas, and, thus, δ^2H of methane can eventually become higher than the original δ^2H value. The inversion of carbon isotopes does not necessarily indicate inorganic gases. Similarly, the inversion of hydrogen isotopes does not necessarily indicate inorganic gases.

(3) Hydrogen isotopic fractionation during gas formation can be satisfactorily described by a chemical kinetic model. Compared with the small difference in the distribution of activation energies for the generation of ^{12}C- and ^{13}C-methane obtained from the carbon isotopic fractionation model (generally $E^{13}C_1 - E^{12}C_1 < 1$ kJ/mol), the difference in the reaction fractions corresponding to the activation energies of H- and ^2H-methane is larger ($E^2H_1 - EH_1 > 2$ kJ/mol). The amount of regular methane in the low activation energy region is significantly higher than that of ^2H-containing methane, while the amount of ^2H-methane in the high activation energy region is higher. This leads to more hydrogen isotopic fractionation, which is the reason that the

hydrogen isotopic composition is very sensitive to changes in temperature (maturity).

Acknowledgements

We thank the National Natural Science Foundation of China (41672130, 41772131), the National Oil and Gas Major Project

Appendix Table 1
Hydrogen Isotopic Values of the Main Pyrolysis Products

Experiment	Temperature, °C	Heating rate, °C/h	δ^2H of C_1, ‰ SMOW	δ^2H of C_2, ‰ SMOW	δ^2H of C_3, ‰ SMOW
n-Octadecanen	408.90	20	n.d.	n.d.	n.d.
	432.30	20	−280.90	−243.20	−179.85
	456.80	20	−231.75	−178.39	−123.29
	483.70	20	−190.69	−121.89	−74.51
	504.70	20	−166.81	−76.17	−28.09
	528.00	20	−145.38	−32.48	22.60
	552.00	20	−118.41	9.08	58.76
	576.20	20	−84.34	16.04	n.d.
	600.10	20	−68.22	−5.21	n.d.
	624.00	20	−60.49	−20.27	n.d.
	408.90	2	n.d.	n.d.	n.d.
	432.30	2	−209.51	−157.21	−123.33
	456.80	2	−179.39	−98.01	−59.41
	483.70	2	−158.33	−33.98	−9.30
	504.70	2	−124.94	3.19	47.16
	528.00	2	−88.02	14.31	17.40
	552.00	2	−62.32	13.02	n.d.
	576.20	2	−47.67	−15.08	n.d.
	600.10	2	−43.62	−31.55	n.d.
	624.00	2	−26.84	n.d.	n.d.
Octadecylamine	408.90	20	n.d.	n.d.	n.d.
	432.30	20	−337.36	−331.53	−316.84
	483.70	20	−351.22	−303.48	−267.90
	504.70	20	−342.01	−266.72	−230.06
	528.00	20	−324.94	−228.84	−180.71
	552.00	20	−294.34	−163.16	n.d.
	576.20	20	−278.41	−172.22	n.d.
	600.10	20	−261.18	−172.69	n.d.
	624.00	20	−254.50	n.d.	n.d.
	408.90	2	−358.79	−353.84	−320.38
	432.30	2	−368.82	−338.07	−297.57
	456.80	2	−355.71	−300.38	−263.62
	483.70	2	−335.03	−238.73	−208.42
	504.70	2	−312.56	−201.31	−200.39
	528.00	2	−285.06	−177.94	−223.39
	552.00	2	−260.83	−168.47	n.d.
	576.20	2	−250.07	−179.74	n.d.
	600.10	2	−241.93	−156.62	n.d.
	624.00	2	−241.71	−133.32	n.d.
n-Octadecanoic acid	408.90	20	−294.57	−362.87	n.d.
	432.30	20	−308.25	−346.21	−229.43
	456.80	20	−320.44	−318.89	−275.91
	483.70	20	−316.15	−281.82	−250.95
	504.70	20	−306.77	−247.10	−209.29
	528.00	20	−302.40	−219.22	−175.36
	552.00	20	−272.06	−180.49	−120.54
	576.20	20	−249.90	−174.77	−177.93
	600.10	20	−231.66	−180.52	n.d.
	624.00	20	−220.75	−192.51	n.d.
	408.90	2	−318.50	−342.45	−281.04
	432.30	2	−325.47	−303.87	−263.35
	456.80	2	−315.08	−261.85	−223.40
	483.70	2	−306.77	−247.10	−201.24
	504.70	2	−281.04	−191.39	−127.31
	528.00	2	−250.59	−169.22	−71.13
	552.00	2	−232.19	−172.34	n.d.
	576.20	2	−212.26	−173.40	n.d.
	600.10	2	−199.18	−174.97	n.d.
	624.00	2	−188.02	−177.22	n.d.
Decahydronaph Thalene	408.90	20	n.d.	n.d.	n.d.
	432.30	20	−199.05	−94.72	−143.58
	456.80	20	−294.27	−222.67	−202.31
	483.70	20	−313.63	−243.40	−217.65
	504.70	20	−261.19	−189.36	−152.65

Appendix Table 1 (*continued*)

Experiment	Temperature, °C	Heating rate, °C/h	δ^2H of C_1, ‰ SMOW	δ^2H of C_2, ‰ SMOW	δ^2H of C_3, ‰ SMOW
	528.00	20	−223.20	−129.87	−99.81
	552.00	20	−194.40	−76.70	−33.17
	576.20	20	−171.77	−48.12	n.d.
	600.10	20	−144.20	−31.11	n.d.
	624.00	20	−134.98	−58.17	n.d.
	408.90	2	−189.57	−138.38	−168.51
	432.30	2	−301.52	−250.97	−221.59
	456.80	2	−310.61	−253.08	−220.83
	483.70	2	−247.33	−157.61	−133.53
	504.70	2	−203.63	−106.15	−90.20
	528.00	2	−170.00	−67.38	−49.75
	552.00	2	−143.07	−44.02	n.d.
	576.20	2	−121.31	−29.28	n.d.
	600.10	2	−108.36	n.d.	n.d.
	624.00	2	−104.06	n.d.	n.d.
9-Phenylanthracene	408.90	20	n.d.	n.d.	n.d.
	432.30	20	n.d.	n.d.	n.d.
	456.80	20	n.d.	n.d.	n.d.
	483.70	20	−145.82	−65.08	n.d.
	504.70	20	−101.34	20.04	n.d.
	528.00	20	−73.38	73.68	n.d.
	552.00	20	−32.57	91.51	n.d.
	576.20	20	−9.89	n.d.	n.d.
	600.10	20	21.70	n.d.	n.d.
	624.00	20	44.28	n.d.	n.d.
	408.90	2	n.d.	n.d.	n.d.
	432.30	2	n.d.	n.d.	n.d.
	456.80	2	−109.16	n.d.	n.d.
	483.70	2	−77.29	19.02	n.d.
	504.70	2	−31.89	77.82	n.d.
	528.00	2	3.25	102.80	n.d.
	552.00	2	29.99	n.d.	n.d.
	576.20	2	46.80	n.d.	n.d.
	600.10	2	79.96	n.d.	n.d.
	624.00	2	104.21	n.d.	n.d.

n.d. — not detected.

(2016ZX05061-003-001, 2016ZX05029002-002), the Sinopec Scientific and Technological Research Project (P17027-3), and the Ministry of Education's Independent Innovation Fund Project (14CX02224A) for financial support of this study. We also thank Jinzhong Liu at Research Institute of Guangzhou, Institute of Geochemistry, Chinese Academy of Sciences, for his help and support.

Appendix Table 2. Activation Energy Distributions of Model Compounds

Activation energy, kJ/mol	Reaction fraction									
	n-Octadecane		n-Octadecanoic acid		Octadecylamine		Decahydronaphthalene		9-Phenylanthracene	
	CH_4	CH_3^2H	CH_4	CH_3^2H	CH_4	CH_3^2H	CH_4	CH_3^2H	CH_4	CH_3^2H
150	0.0000	0.0000	0.0000	0.0000	0.0000	0.0000	0.0000	0.0000	0.0000	0.0000
160	0.0000	0.0000	0.0000	0.0000	0.0000	0.0000	0.0000	0.0000	0.0000	0.0000
170	0.0000	0.0000	0.0000	0.0000	0.0000	0.0001	0.0000	0.0000	0.0000	0.0000
180	0.0000	0.0000	0.0000	0.0000	0.0000	0.0000	0.0000	0.0000	0.0000	0.0000
190	0.0000	0.0000	0.0000	0.0000	0.0000	0.0000	0.0000	0.0000	0.0000	0.0000
200	0.0000	0.0000	0.0000	0.0000	0.0000	0.0005	0.0000	0.0000	0.0000	0.0000
210	0.0000	0.0000	0.0000	0.0000	0.0000	0.0000	0.0000	0.0005	0.0000	0.0000
220	0.0000	0.0000	0.0000	0.0000	0.0000	0.0000	0.0000	0.0005	0.0000	0.0000
230	0.0000	0.0000	0.0000	0.0000	0.0000	0.0000	0.0000	0.0000	0.0000	0.0000
240	0.1258	0.0740	0.2120	0.1600	0.1573	0.1133	0.0000	0.0000	0.2198	0.1358
250	0.2636	0.2780	0.1766	0.1571	0.2116	0.1979	0.3231	0.1971	0.4655	0.3983
260	0.3234	0.2127	0.3203	0.2806	0.3232	0.2889	0.3170	0.3840	0.0000	0.0335
270	0.1146	0.2548	0.1339	0.1878	0.1484	0.2068	0.1791	0.1734	0.1946	0.1906
280	0.1535	0.0819	0.0958	0.0817	0.0794	0.0787	0.1537	0.1514	0.0845	0.1011
290	0.0000	0.0632	0.0380	0.0936	0.0685	0.1060	0.0000	0.0713	0.0000	0.0245
300	0.0192	0.0151	0.0207	0.0220	0.0117	0.0000	0.0272	0.0119	0.0354	0.0890
310	0.0000	0.0206	0.0028	0.0174	0.0000	0.0077	0.0000	0.0000	0.0004	0.0000
320	0.0000	0.0000	0.0000	0.0000	0.0000	0.0000	0.0000	0.0100	0.0000	0.0000
330	0.0000	0.0000	0.0000	0.0000	0.0000	0.0000	0.0000	0.0000	0.0000	0.0000
340	0.0000	0.0000	0.0000	0.0000	0.0000	0.0000	0.0000	0.0000	0.0000	0.0271

References

Berner, U., Faber, E., Scheeder, G., et al., 1995. Primary cracking of algal and landplant kerogens: kinetic models of isotope variations in methane, ethane and propane. Chem. Geol. 126 (3–4), 233–245. https://doi.org/10.1016/0009-2541(95)00120-4.

Botz, R., Pokojski, H.D., Schmitt, M., et al., 1996a. Carbon isotope fractionation during bacterial methanogenesis by CO_2, reduction. Org. Geochem. 25 (3–4), 255–262. https://doi.org/10.1016/s0146-6380(96)00129-5.

Botz, R., Stüben, D., Winckler, G., et al., 1996b. Hydrothermal gases offshore milos island, Greece. Chem. Geol. 130 (3), 161–173. https://doi.org/10.1016/0009-2541(96)00023-x.

Burnham, A.K., Schmidt, B.J., Braun, R.L., 1995. A test of the parallel reaction model using kinetic measurements on hydrous pyrolysis residues. Org. Geochem. 23 (10), 931–939. https://doi.org/10.1016/0146-6380(95)00069-0.

Cai, C.F., Cai, L.L., Zhang, J., et al., 2013. H_2S-generation by methane-dominated TSR and carbon isotope fractionation in lower triassic feixianguan formation, northeast sichuan basin. In: Annual (Twelfth) Annual (2012) Annual Meeting of the Institute of Geology and Geophysics of the Chinese Academy of Sciences.

Carpentier, B., Ungerer, P., Kowalewski, I., et al., 1996. Molecular and isotopic fractionation of light hydrocarbons between oil and gas phases. Org. Geochem. 24 (12), 1115–1139. https://doi.org/10.1016/s0146-6380(96)00097-6.

Cifuentes, L.A., Salata, G.G., 2001. Significance of carbon isotope discrimination between bulk carbon and extracted phospholipid fatty acids in selected terrestrial and marine environments. Org. Geochem. 32 (4), 613–621. https://doi.org/10.1016/s0146-6380(00)00198-4.

Cramer, B., Krooss, B.M., Littke, R., 1998. Modelling isotope fractionation during primary cracking of natural gas: a reaction kinetic approach. Chem. Geol. 149 (3–4), 235–250. https://doi.org/10.1016/s0009-2541(98)00042-4.

Cramer, B., Faber, E., Gerling, P., et al., 2001. Reaction kinetics of stable carbon isotopes in natural gas–Insights from dry, open system pyrolysis experiments. Energy Fuel. 15 (3), 517–532. https://doi.org/10.1016/s0140-6701(02)85336-x.

Dai, J.X., Qi, H.F., Hao, S.S., 1989. Natural Gas Geology. Petroleum industry press, Beijing (in Chinese).

Dai, J.X., Song, Y., Sun, Y.X., 1993. Coal formed gas in the turpan hami basin. Petrol. Explor. Dev. 20 (2), 6~10 (in Chinese).

Gaschnitz, R., Krooss, B.M., Gerling, P., et al., 2001. On-line pyrolysis-GC-IRMS: isotope fractionation of thermally generated gases from coals. Fuel 80 (15), 2139–2153. https://doi.org/10.1016/s0016-2361(01)00095-3.

Guan, P., Wu, T.H., 2003. Formation mechanism of carbon isotopic distribution of methane in thermal genesis. Acta Sedimentol. Sin. 21 (1), 175–182 (in Chinese).

Guo, W.F., Mosenfelder, J.L., Goddard III, W.A., et al., 2009. Isotopic fractionations associated with phosphoric acid digestion of carbonate minerals: insights from first-principles theoretical modeling and clumped isotope measurements. Geochem. Cosmochim. Acta 73 (24), 7203–7225. https://doi.org/10.1016/j.gca.2009.05.071.

He, K., Zhang, S.C., Mi, J.K., et al., 2018. The evolution of chemical groups and isotopic fractionation at different maturation stages during lignite pyrolysis. Fuel 211, 492–506. https://doi.org/10.1016/j.FUEL.2017.09.085.

He, K., Zhang, S.C., Mi, J.K., 2019. Carbon and hydrogen isotope fractionation for methane from non-isothermal pyrolysis of oil in anhydrous and hydrothermal conditions. Energy Explor. Exploit. 37 (5), 1558–1576. https://doi.org/10.1177/0144598719857189.

Jin, Y.B., Wilkins, R.W.T., Tang, Y.C., 2010. A kinetic model of stable carbon isotope ratios in gaseous hydrocarbons generated from thermal cracking of n-tetracosane and its application to the Tarim Basin. J. Petrol. Sci. Eng. 70 (1–2), 44–51. https://doi.org/10.1016/j.petrol.2009.08.013.

Landais, P., Michels, R., Elie, M., 1994. Are time and temperature the only constraints to the simulation of organic matter maturation? Org. Geochem. 22 (3–5), 617–630. https://doi.org/10.1016/0146-6380(94)90128-7.

Li, J.J., Lu, S.F., Xue, H.T., 2008. Migration and accumulation efficiency of natural gas in feixiangnan formation oolitic gas reservoirs, Northeastern Sichuan Basin, 2008 Earth Sci. J. China Univ. Geosci. 33 (4), 565–571 (in Chinese).

Liu, J.Z., Tang, Y.C., 1998. A case of methane generation predicted by the kinetic method of kerogen hydrocarbon generation. Chin. Sci. Bull. 43 (11), 1187–1191 (in Chinese).

Liu, J.Z., Tang, Y.C., 2000. Experimental study on the formation of n-alkanes in coal. Prog. Nat. Sci. 10 (12), 1131–1135 (in Chinese).

Liu, Q.Y., Jin, Z.J., Wang, X.F., et al., 2018. Distinguishing kerogen and oil cracked shale gas using H, C-isotopic fractionation of alkane gases. Mar. Petrol. Geol. 91, 350–362. https://doi.org/10.1016/j.marpetgeo.2018.01.006.

Lorant, F., Prinzhofer, A., Behar, F., et al., 1998. Carbon isotopic and molecular constraints on the formation and the expulsion of thermogenic hydrocarbon gases. Chem. Geol. 147 (3–4), 249–264. https://doi.org/10.1016/s0009-2541(98)00017-5.

Lorant, F., Behar, F., Vandenbroucke, M., et al., 2000. Methane generation from methylated aromatics: kinetic study and carbon isotope modeling. Energy Fuel. 14 (6), 1143–1155. https://doi.org/10.1021/ef990258e.

Lu, S.F., Li, J.J., Xue, H.T., et al., 2006. Comparative study of carbon isotope fractionation model. Nat. Gas. Ind. 26 (7), 1–4 (in Chinese).

Lu, S.F., Wang, M., Xue, H.T., et al., 2011. The impact of aqueous medium on gas yields and kinetic behaviors of hydrogen isotope fractionation during organic matter thermal degradation. Acta Geol Sin-Engl. 85 (6), 1466–1477. https://doi.org/10.1111/j.1755-6742.2011.00599.x.

Lu, J.M., Larson, T.E., Smyth, R.C., 2015. Carbon isotope effects of methane transport through anahuac shale - a core gas study. J. Geochem. Explor. 148, 138–149. https://doi.org/10.1016/j.gexplo.2014.09.005.

Lu, S.F., Li, J.J., Xue, H.T., et al., 2019. Pyrolytic gaseous hydrocarbon generation and the kinetics of carbon isotope fractionation in representative model compounds with different chemical structures. G-cubed 20, 1–21. https://doi.org/10.1029/2018GC007722.

Mazeas, L., Budzinski, H., 2002. Molecular and stable carbon isotopic source identification of oil residues and oiled bird feathers sampled along the atlantic coast of France after the erika oil spill. Environ. Sci. Technol. 36 (2), 130–137. https://doi.org/10.1021/es010726a.

Métayer, P.L., Grice, K., Chow, C.N., et al., 2014. The effect of origin and genetic processes of low molecular weight aromatic hydrocarbons in petroleum on their stable carbon isotopic compositions. Org. Geochem. 72, 23–33. https://doi.org/10.1016/j.orggeochem.2014.04.008.

Ni, Y.Y., Ma, Q.S., Ellis, G.S., et al., 2011. Fundamental studies on kinetic isotope effect (KIE) of hydrogen isotope fractionation in natural gas systems. Geochem. Cosmochim. Acta 75 (10), 2696–2707. https://doi.org/10.1016/j.gca.2011.02.016.

Ni, Y.Y., Dai, J.X., Zhu, G.Y., et al., 2013. Stable hydrogen and carbon isotopic ratios of coal-derived and oil-derived gases: a case study in the Tarim basin, NW China. Int. J. Coal Geol. 116–117, 302–313. https://doi.org/10.1016/j.coal.2013.06.006.

Peters, K.E., Walters, C.C., Moldowan, J.M., 2005. The biomarker guide. Biomarkers & Isotopes in Petroleum Systems & Earth History Ed. 2, 490.

Redding, C.E., Schoell, M., Monin, J.C., et al., 1980. Hydrogen and carbon isotopic composition of coals and kerogens. Phys. Chem. Earth 12 (79), 711–723. https://doi.org/10.1016/0079-1946(79)90152-6.

Rooney, M.A., Claypool, G.E., Chung, H.M., 1995. Modeling thermogenic gas generation using carbon isotope ratios of natural gas hydrocarbons. Chem. Geol. 126 (3–4), 219–232. https://doi.org/10.1016/0009-2541(95)00119-0.

Sajgó, C., Mcevoy, J., Wolff, G.A., et al., 1986. Influence of temperature and pressure on maturation processes—i. preliminary report. Org. Geochem. 10 (1), 331–337. https://doi.org/10.1016/0146-6380(86)90033-1.

Schenk, H.J., Dieckmann, V., 2004. Prediction of petroleum formation: the influence of laboratory heating rates on kinetic parameters and geological extrapolations. Mar. Petrol. Geol. 21 (1), 79–95. https://doi.org/10.1016/j.marpetgeo.2003.11.004.

Schenk, H.J., Primio, R.D., Horsfield, B., 1997. The conversion of oil into gas in petroleum reservoirs. part 1: comparative kinetic investigation of gas generation from crude oils of lacustrine, marine and fluviodeltaic origin by programmed-temperature closed-system pyrolysis. Org. Geochem. 26 (7), 467–481. https://doi.org/10.1016/s0146-6380(97)00024-7.

Shuai, Y.H., Zou, Y.R., Peng, P.A., 2003. Kinetics modeling of stable carbon isotopes of coal-generated methane and its significance for gases accumulation in the Kuqa Depression. Tarim Basin. Geochimica. 32 (5), 469–475. https://doi.org/10.3321/j.issn:0379-1726.2003.05.008 (in Chinese).

Stahl, W., 1974. Carbon isotope fractionation in natural gases. Nature 251 (5471), 134–135. https://doi.org/10.1038/251134a0.

Tang, Y.C., Perry, J.K., Jenden, P.D., et al., 2000. Mathematical modeling of stable carbon isotope ratios in natural gases. Geochem. Cosmochim. Acta 64 (15), 2673–2687. https://doi.org/10.1016/s0016-7037(00)00377-x.

Tang, Y.C., Huang, Y.S., Ellis, G.S., et al., 2005. A kinetic model for thermally induced hydrogen and carbon isotope fractionation of individual n-alkanes in crude oil. Geochem. Cosmochim. Acta 69 (18), 4505–4520. https://doi.org/10.1016/j.gca.2004.12.026.

Ungerer, P., 1990. State of the art of research in kinetic modeling of oil formation and expulsion. Org. Geochem. 16 (1–3), 1–25. https://doi.org/10.1016/0146-6380(90)90022-R.

Wang, W.C., 1996. Geochemical characteristics of hydrogen isotopes of natural gas, oil and kerogen. Acta Sedimentol. Sin. 131–135 (in Chinese).

Wang, X.F., Liu, W.H., Liu, Q.Y., et al., 2004. Advance in research on hydrogen isotopic geochemistry of organism and its depositional evolving products. Nat Gas Geosci 15 (3), 311–316 (in Chinese).

Wang, X.F., Liu, W.H., Shi, B.G., et al., 2015. Hydrogen isotope characteristics of thermogenic methane in Chinese sedimentary basins. Org. Geochem. 83–84, 178–189. https://doi.org/10.1016/j.orggeochem.2015.03.010.

Xia, X.Y., Tang, Y.C., 2012. Isotope fractionation of methane during natural gas flow with coupled diffusion and adsorption/desorption. Geochem. Cosmochim. Acta 77 (1), 489–503. https://doi.org/10.1016/j.gca.2011.10.014.

Xia, X.Y., Ellis, G.S., Ma, Q.S., et al., 2014. Compositional and stable carbon isotopic fractionation during non-autocatalytic thermochemical sulfate reduction by gaseous hydrocarbons. Geochem. Cosmochim. Acta 139, 472–486. https://doi.org/10.1016/j.gca.2014.05.004.

Xiong, Y.Q., Geng, A.S., Wang, Y.P., et al., 2001. Experimental study on kinetic simulation of two secondary hydrocarbon generation of kerogen. Sci. China, Ser. A D 31 (4), 315–320 (in Chinese).

Xu, Y.C., Fu, J.M., Zheng, J.J., 2000. The Genesis of Natural Gas and the Geoscience Foundation of Large and Medium Gas Fields. Science Press. 2000., Beijing (in Chinese).

Zhang, Y.G., 1991. Accumulation and Preservation of Natural Gas. Hehai University Press, Nanjing (in Chinese).

Zhang, S.C., He, K., Hu, G.Y., et al., 2018. Unique chemical and isotopic characteristics and origins of natural gases in the Paleozoic marine formations in the Sichuan Basin, SW China: isotope fractionation of deep and high mature carbonate reservoir gases. Mar. Petrol. Geol. 81 (1), 68–82. https://doi.org/10.1016/j.marpetgeo.2017.02.010.

Zou, Y.R., Shuai, Y.H., Kong, F., et al., 2003. Mathematic models of stable carbon isotope composition of coal-derived methane and their applications. Nat Gas Geosci 14 (2), 92–96 (in Chinese).